# Mortality can produce limit cycles in density-dependent models with a predator-prey relationship

Tahani Mtar, Radhouane Fekih-Salem, Tewfik Sari

# MORTALITY CAN PRODUCE LIMIT CYCLES IN DENSITY-DEPENDENT MODELS WITH A PREDATOR-PREY RELATIONSHIP

Tahani Mtar[a] and Radhouane Fekih-Salem[a,c,*] and Tewfik Sari[b]

[a]University of Tunis El Manar, National Engineering School of Tunis, LAMSIN, 1002, Tunis, Tunisia
[b] ITAP, Univ Montpellier, INRAE, Institut Agro, Montpellier, France
[c] University of Monastir, Higher Institute of Computer Science of Mahdia, 5111, Mahdia, Tunisia

Abstract. In this paper, we study an interspecific density-dependent model of two species competing on a single nutrient in a chemostat, taking into account the predator-prey relationship. Without mortality of species, we have proved previously that the system may have a multiplicity of positive steady states that can only appear or disappear through saddle-node or transcritical bifurcations. Including the mortality, we give a complete analysis for the existence and local stability of all steady states of the three-dimensional system which cannot be reduced to a two-dimensional one. We highlight the effect of mortality to destabilize the positive steady state with the emergence of stable limit cycles through supercritical Hopf bifurcations. To describe how the process behaves according to control parameters represented by the dilution rate and the input concentration of the substrate, we determine theoretically the operating diagram by plotting the various conditions of existence and stability and numerically by using MATCONT. The bifurcation diagram according to the input concentration shows the various types of bifurcations of steady states and the coexistence either around a positive steady state or sustained oscillations.

1. **Introduction.** The chemostat is an important laboratory apparatus used for continuous cultures of microorganisms in microbiology and ecology. The mathematical analysis of the classical chemostat model of two or more microbial species competing for a single limiting nutrient shows that only the species with the lowest 'break-even' concentration survives while all other species are extinct (see, for instance, [21, 40]). This result, known as the Competitive Exclusion Principle (CEP), has a long history in the literature of bio-mathematics and recently in [35] a new proof of this principle is given using elementary analysis and comparisons of solutions of ordinary differential equations.

Despite the CEP has been confirmed by the experiences of Hansen and Hubbell [20], this principle contradicts the great biodiversity found in nature as well as

2010 *Mathematics Subject Classification.* Primary: 34A34, 34D20; Secondary: 92B05, 92D25.
*Key words and phrases.* Density-dependence; Hopf Bifurcation; limit cycle; mortality; operating diagram; predator-prey relationship.
The first author thanks the Tunisian Ministry of Higher Education, Scientific Research and Technology for financial support and INRAE for hosting her in Montpellier during the preparation of this work. This work was supported by the Euro-Mediterranean research network TREASURE (https://www6.inrae.fr/treasure/).
* Corresponding author: Radhouane Fekih-Salem.

bioprocesses. To better reconcile theory and observations, several recent extensions of this classic chemostat model have been triggered promoting the coexistence of microbial species. The reader can found in the existing literature the following various coexistence mechanisms: the intra and inter specific competition [1, 9], the flocculation [14, 16, 17, 18, 19], the density-dependence of the growth functions [7, 15, 22, 27, 28, 29, 30, 33], the predator-prey interactions [6, 26], the complex food webs [2, 23, 45], the presence of inhibitors that affects the strongest competitor [3, 10, 11], the commensalistic relationship [4, 5, 37], and the syntrophic relationship [8, 13, 36, 46].

An extension of the classical chemostat model was considered in a series of papers by Lobry et al. [22, 27, 28, 29, 30], taking into account general intra and interspecific density-dependent growth rates with distinct removal rates for each species. Considering particular density-dependent growth functions with intraspecific interference, the numerical simulations in [27] show the coexistence between several species for small enough inter specific interference and the exclusion of one species, at least, for large enough inter specific interference. In [15], a mathematical analysis confirms these numerical results where this system presents the global stability of the coexistence steady state for small enough interspecific interference terms while this system exhibits bi-stability for large enough interspecific interference. With the same removal rates and only interspecific interferences, the coexistence of two species is impossible which confirms the CEP [12].

The present paper considers a model of two competitors for a single resource in a chemostat, with interspecific density-dependent growth functions. The species have a predator-prey relationship, that is, the first species (the prey) promotes the growth of the second species (the predator) which in turn inhibits the growth of the first species. In our study, the mortality (or decay) of two species is taken into account and not neglected as in previous studies [12, 33]. The model can be written as follows:

$$\left\{\begin{array}{lcl} \dot{S} &=& D(S_{in}-S)-f_1(S,x_2)x_1-f_2(S,x_1)x_2,\\ \dot{x}_1 &=& (f_1(S,x_2)-D_1)x_1,\\ \dot{x}_2 &=& (f_2(S,x_1)-D_2)x_2, \end{array}\right. \tag{1}$$

where $S$ is the substrate concentration; $x_1(t)$ and $x_2(t)$ are, respectively, the concentrations of prey and predator species; $D$ and $S_{in}$ are, respectively, the dilution rate and the input substrate concentration in the chemostat; $f_1$ is the density-dependent growth rate of the prey species $x_1$ that is assumed to be increasing in the variable $S$ and decreasing in the predator species $x_2$; $f_2$ is the density-dependent growth rate of the predator species $x_2$ that is assumed to be increasing in the variable $S$ and increasing in the prey species $x_1$; $D_i$, $i=1,2$ is the removal rate of species $x_i$ and can be modeled as in [17, 39] by

$$D_i=\alpha_i D+a_i,\quad i=1,\dots,n \tag{2}$$

where the coefficient $\alpha_i$ belongs to $[0,1]$ and represents the fraction of the prey and predator species leaving the reactor as proposed by [5] to model a biomass reactor attached to the support or to decouple the residence time of solids and the hydraulic residence time $(1/D)$; $a_i$ is the nonnegative mortality (or decay) rate of the species $x_i$.

In [12, 33], the mathematical analysis of model (1) shows that the system may exhibit the coexistence or the bi-stability with a multiplicity of positive steady states, in the particular case $\alpha_i=1$ and $a_i=0$. Moreover, in [33], the operating

diagram shows that all steady states can appear or disappear only through saddle-node or transcritical bifurcations according to the control parameters represented by the dilution rate and the input concentration of the substrate. Indeed, the operating diagram is a very useful tool to determine how a process behaves when all biological parameters are fixed and the control parameters are varied, as they are the most easily parameters to manipulate in a chemostat. It is studied either numerically as in [24, 37, 43, 44, 46] or theoretically as in [1, 3, 8, 11, 10, 15, 18, 21, 33, 36]. In [34], we have studied the existence and the local stability of model (1) in the particular cas where $\alpha_i = 1$.

The aim of this paper is to understand the joined effect of mortality and predator-prey relationship on the behavior of the density-dependent model considered in [12, 33]. In this work, our study provides an extension of the results in [12, 33] by considering distinct removal rates where the system cannot be reduced to a two-dimensional one. Using the Routh–Hurwitz criterion, we determine the existence conditions of all steady states and their local stability according to operating parameters. In contrast to the case without mortality where the coexistence may occur only around a positive steady state [12, 33], our results show that the mortality can destabilize the positive steady state through Hopf bifurcation where the coexistence can be around a stable limit cycle. It is known that introducing decay for the species in the classical predator-prey models in the chemostat results in instability and chaos [25]. For more details on food-chains in the chemostat, the reader may consult [6, 41, 42]. In our model, the same intrinsic effect of mortality on the stability of the positive steady state is observed. Indeed, when mortality is included in the density-dependent model with predator-prey relationship, the positive steady state is not necessarily stable, when it exists. On the other hand, our study provides an important tool for the experimentation which is the operating diagram where we succeed to determine the region of the emergence of stable limit cycles theoretically from Routh–Hurwitz conditions and numerically by using the software MATCONT [32]. Finally, a one-parameter bifurcation diagram determines all types of bifurcations.

The paper is structured as follows. We first introduce in Section 2 assumptions on the growth functions and preliminary results. Then, we determine the necessary and sufficient conditions of existence and stability of the steady states using the null-cline method. In Section 3, we determine theoretically the operating diagrams and then numerically by using MATCONT. In Section 4, we study the one-parameter bifurcation diagram with respect to the input concentration $S_{in}$. The numerical simulations validate the theoretical analysis of the operating diagram. Some conclusions are drawn in Section 5. All the proofs are reported in A. In Appendix B, we construct the operating diagram. In Appendix C, a numerical study of the Hopf bifurcation is provided with respect to $S_{in}$. Finally, all the parameter values used in simulations are provided in Appendix D.

## 2. **Assumptions and mathematical analysis.**

In this paper, we assume that the growth function $f_i(S, x_j)$, $i = 1, 2$, $j = 1, 2$, $i \neq j$ is continuously differentiable ($\mathcal{C}^1$) and satisfies the following hypotheses.

(H1) For all $x_j \geqslant 0$ and $S > 0$, $f_i(0, x_j) = 0$ and $f_2(S, 0) = 0$.

(H2) For all $S > 0$, $x_1 > 0$ and $x_2 \geqslant 0$, $\frac{\partial f_i}{\partial S}(S, x_j) > 0$, $\frac{\partial f_1}{\partial x_2}(S, x_2) < 0$ and $\frac{\partial f_2}{\partial x_1}(S, x_1) > 0$.

Assumption (H1) means that the substrate is necessary for the growth of each species and the prey species $x_1$ is necessary for the growth of the predator species $x_2$. Assumption (H2) means that the growth rate of the prey species $x_1$ is increases with the concentration of the substrate $S$ and is inhibited by the second species $x_2$. While the growth of the predator species $x_2$ is increasing with the concentration of the substrate $S$ and the prey species $x_1$. We now prove the following result.

**Proposition 1.** *Assume that assumptions (H1)-(H2) hold. For any nonnegative initial condition, the solution of system (1) exists for all $t \geqslant 0$, remains nonnegative and is bounded. In addition, the set*

$$\Omega = \left\{(S, x_1, x_2) \in \mathbb{R}^3_+ : S + x_1 + x_2 \leqslant DS_{in}/D_{\min}\right\}$$

*is positively invariant and is a global attractor for the dynamics (1), where* $D_{\min} = \min(D, D_1, D_2)$.

Now, we shall discuss the existence of steady states of system (1) and then their asymptotic stability. A steady state of (1) exists or is said to be 'meaningful' if and only if all its components are nonnegative. The steady states are given by the solutions of the following system:

$$\begin{cases} 0 &= D(S_{in} - S) - f_1(S, x_2)x_1 - f_2(S, x_1)x_2, \\ 0 &= (f_1(S, x_2) - D_1)x_1, \\ 0 &= (f_2(S, x_1) - D_2)x_2. \end{cases} \tag{3}$$

If $x_1 = 0$ and $x_2 > 0$, we obtain $D_2 = 0$ from assumption (H1), which is impossible. Thus, system (1) can have at most three types of steady states labeled as follows:

- $\mathcal{E}_0$ ($x_1 = x_2 = 0$): the washout of two species which always exists.
- $\mathcal{E}_1$ ($x_1 > 0$, $x_2 = 0$): only prey species is present.
- $\mathcal{E}^*$ ($x_1 > 0$, $x_2 > 0$): the coexistence of two species.

From (H2), the function $S \mapsto f_1(S, 0)$ is increasing. Hence, if $D < (f_1(+\infty, 0) - a_1)/\alpha_1$, then there exists a unique solution $S = \lambda_1(D)$ (called the *break-even concentration*) of equation

$$f_1(S, 0) = \alpha_1 D + a_1. \tag{4}$$

If $D \geqslant (f_1(+\infty, 0) - a_1)/\alpha_1$, we let $\lambda_1(D) = +\infty$. The following result determines the existence condition of the steady state $\mathcal{E}_1$ according to operating parameters.

**Proposition 2.** *Assume that (H1) and (H2) hold. The boundary steady state $\mathcal{E}_1 = (\tilde{S}, \tilde{x}_1, 0)$ of system (1) is defined by*

$$\tilde{S} = \lambda_1(D) \quad \text{and} \quad \tilde{x}_1 = \frac{D}{D_1}(S_{in} - \lambda_1(D)). \tag{5}$$

*It exists if and only if*

$$S_{in} > \lambda_1(D). \tag{6}$$

*When it exists, $\mathcal{E}_1$ is unique.*

In what follows, we determine the existence condition of the positive steady state $\mathcal{E}^* = (S^*, x_1^*, x_2^*)$ where the components $S = S^*$, $x_1 = x_1^*$ and $x_2 = x_2^*$ must be the solutions of (3) with $x_1 > 0$ and $x_2 > 0$. That is, $S^*$, $x_1^*$ and $x_2^*$ are the solutions of the set of equations

$$D(S_{in} - S) = D_1x_1 + D_2x_2 \tag{7}$$

$$f_1(S, x_2) = D_1 \tag{8}$$

$$f_2(S, x_1) = D_2. \tag{9}$$

From (7), the solution $S^*$ is given by

$$S^* = S_{in} - D_1 x_1^*/D - D_2 x_2^*/D. \tag{10}$$

Replacing $S^*$ by this expression in (8,9), we see that $(x_1 = x_1^*, x_2 = x_2^*)$ must be a solution of

$$\begin{cases} \widetilde{f}_1(x_1, x_2) := f_1(S_{in} - D_1 x_1/D - D_2 x_2/D, x_2) - D_1 = 0 \\ \widetilde{f}_2(x_1, x_2) := f_2(S_{in} - D_1 x_1/D - D_2 x_2/D, x_1) - D_2 = 0. \end{cases} \tag{11}$$

Note that the functions $\widetilde{f}_i$, $i = 1, 2$, $j = 1, 2$, $i \neq j$ are defined on the set

$$M := \left\{(x_1, x_2) \in \mathbb{R}_+^2 : D_1 x_1/D + D_2 x_2/D \leqslant S_{in}\right\}.$$

In addition, $S^*$ is positive if and only if $D_1 x_1^*/D + D_2 x_2^*/D < S_{in}$, that is, (11) has a positive solution in the interior $\mathring{M}$ of $M$. In what follows, we define the line $\delta$ by $D_1 x_1/D + D_2 x_2/D = S_{in}$ and we need the next notations:

$$E = \frac{\partial f_1}{\partial S}, \quad F = \frac{\partial f_2}{\partial S}, \quad G = -\frac{\partial f_1}{\partial x_2}, \quad H = \frac{\partial f_2}{\partial x_1}. \tag{12}$$

We have used the opposite sign of the partial derivative $G = -\partial f_1/\partial x_2$, such that all constants involved in the computation become positive. To solve (11) in $\mathring{M}$, we need the following Lemmas 1, 2 and 3 where the proofs are similar to those in [34].

**Lemma 1.** *Assume that assumptions (H1)-(H2) and condition (6) hold. The equation $\widetilde{f}_1(x_1, x_2) = 0$ defines a smooth decreasing function*

$$\begin{array}{rccc} F_1 & : & [0, \tilde{x}_1] & \longrightarrow & [0, \tilde{x}_2] \\ & & x_1 & \longmapsto & F_1(x_1) = x_2, \end{array}$$

*such that $F_1(\tilde{x}_1) = 0$, $F_1(0) = \tilde{x}_2$ and*

$$-\frac{D_1}{D_2} < F_1'(x_1) = -\frac{D_1 E}{D_2 E + G} < 0, \quad \textit{for all} \quad x_1 \in [0, \tilde{x}_1], \tag{13}$$

*where $\tilde{x}_2$ is the unique solution of the equation $\widetilde{f}_1(0, x_2) = 0$. In addition, the graph $\gamma_1$ of $F_1$ lies in $\mathring{M}$, that is, $(x_1, F_1(x_1)) \in \mathring{M}$ for all $x_1 \in (0, \tilde{x}_1)$ (see Fig. 1).*

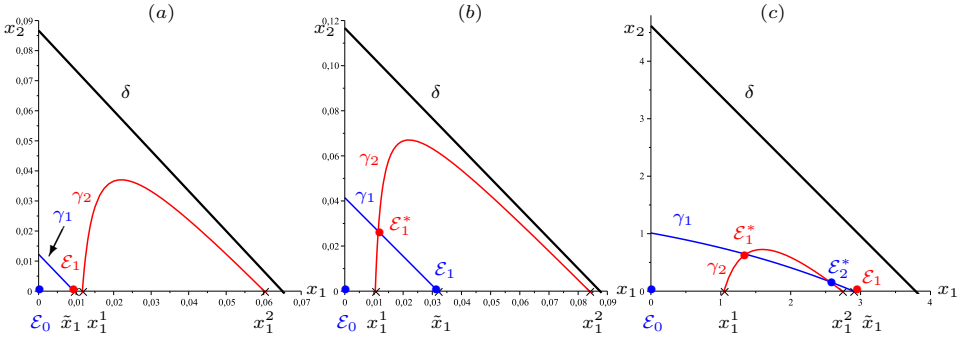


FIGURE 1. Number of positive steady states: (a) Case 1: no positive steady state when $(S_{in}, D) = (0.26, 0.1)$, (b) Case 2: an odd number when $(S_{in}, D) = (0.35, 0.1)$, (*c*) Case 3: an even number when $(S_{in}, D) = (4.5, 0.8)$.

To define the function $x_2 = F_2(x_1)$ of equation $\widetilde{f}_2(x_1, x_2) = 0$, we will need of the following Lemma to determine the necessary and sufficient condition for the existence of solutions of the equation $\widetilde{f}_2(x_1, 0) = 0$.

**Lemma 2.** *Under assumptions (H1)-(H2), the equation $\widetilde{f}_2(x_1,0)=0$ has a solution in $[0,DS_{in}/D_1]$ if and only if,*

$$\max_{x_1\in[0,DS_{in}/D_1]} f_2(S_{in}-D_1x_1/D,x_1)\geqslant D_2. \tag{14}$$

*Generically, we have an even number of solutions in $[0,DS_{in}/D_1]$.*

For simplicity, we add the following assumption which is satisfied by the specific growth rates (22).

(H3) Equation $\widetilde{f}_2(x_1,0)=0$ has at most two solutions $x_1^1$ and $x_1^2$ in $[0,DS_{in}/D_1]$.

The proof of the maximum number of solutions of the equation $\widetilde{f}_2(x_1,0)=0$ for the specific growth rates (22) is similar to that in Appendix B of [34]. When the function $x_1\longmapsto\widetilde{f}_2(x_1,0)$ is multimodal, the study of this general case can be treated similarly, without added difficulty. In this particular case, we obtain the next result.

**Lemma 3.** *Assume that assumptions (H1) to (H3) and condition (14) hold, the equation $\widetilde{f}_2(x_1,x_2)=0$ defines a smooth function*

$$\begin{array}{rccl} F_2 & : & [x_1^1,x_1^2] & \longrightarrow & [0,DS_{in}/D_2[ \\ & & x_1 & \longmapsto & F_2(x_1)=x_2, \end{array}$$

*such that $F_2(x_1^1)=F_2(x_1^2)=0$ and*

$$-\frac{D_1}{D_2}<F_2'(x_1)=-\frac{D_1}{D_2}+\frac{D}{D_2}\frac{H}{F},\quad \textit{for all}\quad x_1\in[x_1^1,x_1^2], \tag{15}$$

*where $x_1^1$ and $x_1^2$ are the solutions of the equation $\widetilde{f}_2(x_1,0)=0$. In addition, the graph $\gamma_2$ of $F_2$ lies in $\mathring{M}$ where $(x_1,F_2(x_1))\in\mathring{M}$ for all $x_1\in(x_1^1,x_1^2)$ (see Fig. 1).*

Applying the previous lemmas, we establish in the following proposition the necessary and sufficient condition of the existence of the coexistence steady state $\mathcal{E}^*$.

**Proposition 3.** *Assume that assumptions (H1) to (H3) and conditions (6) and (14) hold. A positive steady state $\mathcal{E}^*=(S^*,x_1^*,x_2^*)$ of (1) exists if and only if the curves $\gamma_1$ and $\gamma_2$ have a positive intersection, where $S^*$ is given by (10) and $(x_1^*,x_2^*)$ is a positive solution of equations*

$$x_2=F_1(x_1)\quad \textit{and}\quad x_2=F_2(x_1). \tag{16}$$

According to the position of $\tilde{x}_1$ between $x_1^1$ and $x_1^2$, there exist three cases that must be distinguished:

$$\text{Case 1}:\ \tilde{x}_1<x_1^1<x_1^2,\quad \text{Case 2}:\ x_1^1<\tilde{x}_1<x_1^2,\quad \text{Case 3}:\ x_1^1<x_1^2<\tilde{x}_1. \tag{17}$$

When hypotheses (H1)-(H3) and condition (14) hold, one has

$$f_2\left(\lambda_1(D),\frac{D}{D_1}(S_{in}-\lambda_1(D))\right)<D_2\ \Leftrightarrow\ \text{Case 1 or Case 3} \tag{18}$$

$$f_2\left(\lambda_1(D),\frac{D}{D_1}(S_{in}-\lambda_1(D))\right)>D_2\ \Leftrightarrow\ \text{Case 2}. \tag{19}$$

**Remark 1.** 1. Let $S\geqslant 0$. $x_1=\lambda_2(S,y)$ is the unique solution of equation $y=f_2(S,x_1)$. Since the function $x_1\mapsto f_2(S,x_1)$ is increasing, then the function $y\mapsto\lambda_2(S,y)$ is well defined and strictly increasing for $y\in[0,\sup_{x_1\geqslant 0}f_2(S,x_1))$.

2. Condition (18) is equivalent to

$$S_{in} < \lambda_1(D) + \frac{D_1}{D}\lambda_2(\lambda_1(D), D_2) := \varphi(D). \tag{20}$$

Inversely, condition (19) is equivalent to $S_{in} > \varphi(D)$.

As a consequence of the previous results, we obtain the following proposition which determines the multiplicity of positive steady states of (1) according to the three cases of (17) or (equivalently) the two conditions in (18, 19) which depend on the operating parameters (see Fig. 1).

**Proposition 4.** *Assume that hypotheses (H1) to (H3) and conditions (6) and (14) hold.*

1. *In Case 1, there is no positive steady state.*
2. *In Case 2, there exists at least one positive steady state. Generically, the system has an odd number of positive steady states.*
3. *In Case 3, generically system (1) has no positive steady state or an even number of positive steady states.*

Now, we determine the local stability of all steady states of (1) by using the abbreviation LES for Locally Exponentially Stable steady states.

**Proposition 5.** *Assume that assumptions (H1)-(H3) hold.*

1. *$\mathcal{E}_0$ is LES if and only if $S_{in} < \lambda_1(D)$.*
2. *$\mathcal{E}_1$ is LES if and only if $S_{in} < \varphi(D)$.*
3. *$\mathcal{E}^* = (S^*, x_1^*, x_2^*)$ is LES if and only if $F_1'(x_1^*) < F_2'(x_1^*)$ and*

$$\begin{aligned} c_4(D, S_{in}) := {} & D_1E^2x_1^2 + D_2F^2x_2^2 + DD_1Ex_1 + DD_2Fx_2 \\ & + (D_1EF + (D_1 - D)FG + D_2EF + (D - D_2)EH)x_1x_2 \\ & + (EH - FG + GH)(Ex_1^2x_2 + Fx_1x_2^2) > 0. \end{aligned} \tag{21}$$

*where the functions $E$, $F$, $G$ are $H$ are defined by (12), and are evaluated at $\mathcal{E}^*$.*

**Remark 2.** In the particular case without mortality of species ($D_i = D$), the Routh–Hurwitz coefficient given by (21) becomes

$$c_4(D, S_{in}) = D(E^2x_1^2 + F^2x_2^2 + D(Ex_1 + Fx_2)) + 2DEFx_1x_2 + \frac{c_3}{D}(Ex_1 + Fx_2),$$

where the expression of $c_3$ is given by (25). Using the second expression of $c_3$ given by (27), we find the result of [33] in this particular case $D_i = D$ such that the stability of the coexistence steady state $\mathcal{E}^*$ depends on the sign of $F_2'(x_1^*) - F_1'(x_1^*)$ or equivalently the relative positions of the two curves $\gamma_1$ and $\gamma_2$.

The necessary and sufficient conditions of existence and local stability of all steady states of (1) are summarized in Table 1.

TABLE 1. Necessary and sufficient conditions of existence and stability of steady states of system (1) where $c_4$ is defined by (21).

| | Existence | Local stability |
|---|---|---|
| $\mathcal{E}_0$ | always exists | $S_{in} < \lambda_1(D)$ |
| $\mathcal{E}_1$ | $S_{in} > \lambda_1(D)$ | $S_{in} < \varphi(D)$ |
| $\mathcal{E}^*$ | $S_{in} > \varphi(D)$ or $S_{in} < \varphi(D)$ and (16) has a solution | $F_2'(x_1^*) > F_1'(x_1^*)$ and $c_4(D, S_{in}) > 0$ |

3. **Operating diagram.** The aim of this section is to describe theoretically the operating diagram of system (1). We use MAPLE [31] to draw the curves that separate the different regions of existence and stability of the steady states of (1). Then, we use MATCONT [32] to analyse numerically this operating diagram. This diagram allows to understand and classify the qualitative changes of the asymptotic behavior of (1) under variation of the concentration of the substrate in the feed bottle $S_{in}$ and the dilution rate $D$. Since all other parameters in (1) cannot be easily manipulated by the biologist, we fix it as provided in Table 7. To construct the operating diagram, we first define in Table 2 the set of curves $\Upsilon = \{\Upsilon_1, \Upsilon_2, \Upsilon_3\}$ which are the boundaries of different regions of the $(S_{in}, D)$-plane. As stated in the following result, the curves in the set $\Upsilon$ separate the operating plane $(S_{in}, D)$ into four regions, denoted $\mathcal{J}_k$, $k = 1, \ldots, 4$, and defined in Table 3.

TABLE 2. The set of curves $\Upsilon$ and the corresponding colors in Figs. 2 and 3 where $\varphi(D)$ and $c_4$ are defined by (20) and (21), resp.

| $\Upsilon$ | Color |
|---|---|
| $\Upsilon_1 = \{(S_{in}, D) : S_{in} = \lambda_1(D)\}$ | Black |
| $\Upsilon_2 = \{(S_{in}, D) : S_{in} = \varphi(D)\}$ | Blue |
| $\Upsilon_3 = \{(S_{in}, D) : c_4(S_{in}, D) = 0\}$ | Green |

**Proposition 6.** *Assume that assumptions (H1)-(H2) hold and the biological parameter values are provided as of Figs. 2 and 3 in Table 7. The existence and the stability of the steady states of (1) in the four regions $\mathcal{J}_k$, $k = 1, \ldots, 4$ of the operating diagram are determined in Table 3.*

TABLE 3. Existence and stability of steady states according to regions in the operating diagrams of Figs. 2 and 3. The letter S (resp. U) means stable (resp. unstable) steady state. Absence of letter means that the corresponding steady state does not exist.

| Condition | Region | Color | $\mathcal{E}_0$ | $\mathcal{E}_1$ | $\mathcal{E}^*$ |
|---|---|---|---|---|---|
| $S_{in} < \lambda_1(D)$ | $\mathcal{J}_1$ | Cyan | S | | |
| $\lambda_1(D) < S_{in} < \varphi(D)$ | $\mathcal{J}_2$ | Pink | U | S | |
| $\varphi(D) < S_{in}$ and $c_4(S_{in}, D) > 0$ | $\mathcal{J}_3$ | Grey | U | U | S |
| $\varphi(D) < S_{in}$ and $c_4(S_{in}, D) < 0$ | $\mathcal{J}_4$ | Yellow | U | U | U |

To illustrate the operating diagram, we consider the following specific growth rates that satisfying the conditions (H1)-(H2):

$$f_1(S, x_2) = \frac{m_1 S}{K_1 + S} \frac{1}{1 + x_2/L_1}, \quad f_2(S, x_1) = \frac{m_2 S}{K_2 + S} \frac{x_1}{L_2 + x_1}, \tag{22}$$

where $m_1$, $m_2$ are the maximum growth rates; $K_1$, $K_2$ and $L_2$ are the Michaelis-Menten constants; $L_1$ is the inhibition factor due to $x_2$ for the growth of the species $x_1$.

**Remark 3.** To determine the curve $\Upsilon_3$ in the operating diagram of (1), we have used the steady state characteristic method introduced by Lobry et al. [29, 30] that we present in Appendix B. This method is often used to provide a geometric description of the existence and the asymptotic stability of all steady states, see for instance [1, 15, 17].

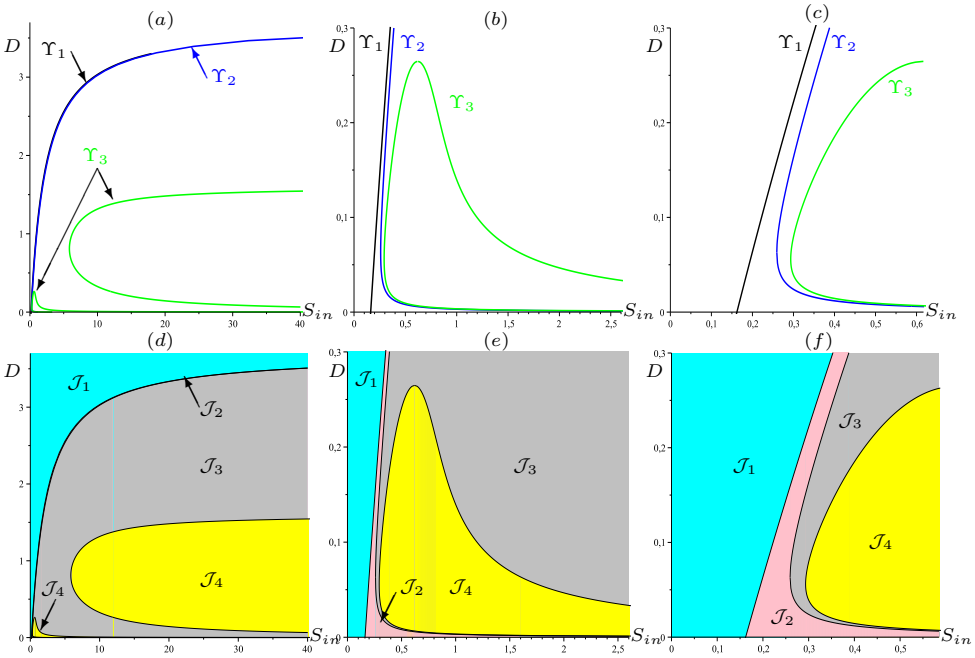


FIGURE 2. Operating diagram of (1) in MAPLE. (b)-(e) Magnification when $(S_{in}, D) \in [0, 2.6] \times [0, 0.3]$. (c)-(f) Magnification when $(S_{in}, D) \in [0, 0.6] \times [0, 0.3]$.

We also used the software MATCONT [32] to determine numerically this operating diagram that we present in Fig. 3. Although it is identical to the theoretical operating diagram in Fig. 2, it must be stressed that they were obtained by completely different methods. The diagram in Fig. 2 is obtained by using our theoretical results and drawing the $\Upsilon_i$ curves, defined in Table 2, that separate the different regions of the operating diagram, whereas the diagram in Fig. 3 is obtained numerically using MATCONT.

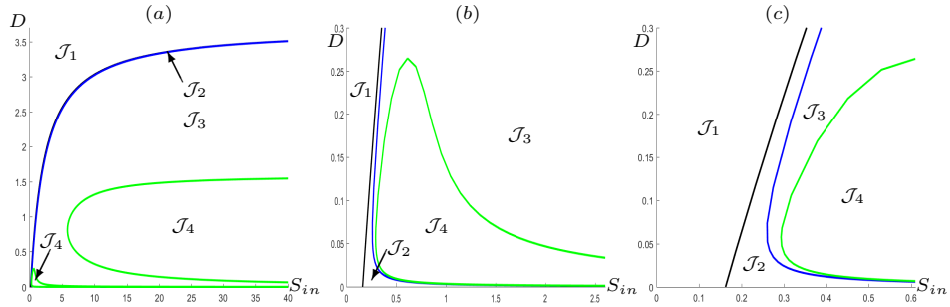


FIGURE 3. Operating diagram of (1) in MATCONT. (b) Magnification when $(S_{in}, D) \in [0, 2.6] \times [0, 0.3]$. (c) Magnification when $(S_{in}, D) \in [0, 0.6] \times [0, 0.3]$.

The following result determines the nature of all types of bifurcations of system (1) that might happen by crossing the various regions of the operating diagrams $(S_{in}, D)$ through the curves of $\Upsilon$ where the steady states coalesce and can change stability.

**Proposition 7.** *The bifurcation analysis of the steady states of (1) by crossing the curves of $\Upsilon$ according to the operating parameters $S_{in}$ and $D$ is summarized in Table 4.*

TABLE 4. Nature of bifurcations of the steady states of (1) by crossing to the surfaces of $\Upsilon$. The letter TB (resp. SHB) means a transcritical bifurcation (resp. Supercritical Hopf bifurcation).

| Curve | Transition | Bifurcation |
|---|---|---|
| $\Upsilon_1$ | $\mathcal{J}_1$ to $\mathcal{J}_2$ | TB: $\mathcal{E}_0 = \mathcal{E}_1$ |
| $\Upsilon_2$ | $\mathcal{J}_2$ to $\mathcal{J}_3$ | TB: $\mathcal{E}_1 = \mathcal{E}^*$ |
| $\Upsilon_3$ | $\mathcal{J}_3$ to $\mathcal{J}_4$ | SHB: $\mathcal{E}^*$ |

Figs. 4(a)-(b) show how the coexistence region around a stable limit cycle $\mathcal{J}_4$ is reduced by decreasing the values of $a_1$ and $a_2$ to 0. For $a_1 = a_2 = 0$, Fig. 4(c) shows the disappearance of this region $\mathcal{J}_4$ which confirms our result in [33] where the process cannot admit a limit cycle without mortality, that is, for same removal rates of species. Therefore, the destabilization of the positive steady state is due to the mortality and is similar to some results obtained in the existing literature on the classical predator-prey model in the chemostat [25].

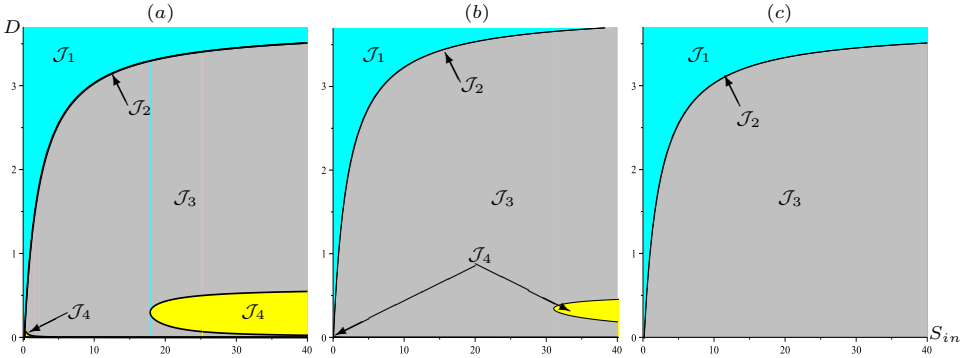


FIGURE 4. Operating diagram of (1) showing the disappearance of the region $\mathcal{J}_4$ when $a_1$ and $a_2$ diminish.

4. **One-parameter bifurcation diagram and numerical simulations.** This section is devoted to study the one-parameter bifurcation diagram of system (1) and to validate our mathematical results in the previous sections by some numerical simulations. First, we determine the bifurcation diagram showing the behavior of the process by varying the input substrate concentration $S_{in}$ as the bifurcating parameter where the dilution rate $D$ is fixed. However, the results are the same regardless of which operating parameter is varied, that is, the end results are similar when we vary the dilution rate $D$. All other parameters of system (1) are fixed (see Table 7). The following result determines the one-parameter bifurcation diagram according to $S_{in}$ from the operating diagram of Fig. 2 (or equivalently of Fig. 3) when the dilution rate $D = 0.25$.

**Proposition 8.** *Assume that the biological parameters in (1) are given as in Table 7 using the specific growth rates (22) with $D = 0.25$. The existence and stability*

*of steady states of (1) according to $S_{in}$ are given in Table 6 where the bifurcation values $\sigma_i$, $i = 1, \ldots, 5$ and the corresponding nature of the bifurcations are defined in Table 5.*

TABLE 5. Definitions of the critical values $\sigma_i$, $i = 1, \ldots, 5$ of $S_{in}$ and the corresponding nature of bifurcations when $D = 0.25$.

| Definition | Value | Bifurcation |
|---|---|---|
| $\sigma_1 = \lambda_1(D)$ | 0.31884 | TB |
| $\sigma_2 = \varphi(D)$ | 0.35394 | TB |
| $\sigma_3$ is the first solution of equation $c_4(S_{in}) = 0$ | 0.52555 | SHB |
| $\sigma_4$ is the second solution of equation $c_4(S_{in}) = 0$ | 0.71593 | SHB |
| $\sigma_5$ is the third solution of equation $c_4(S_{in}) = 0$ | 12.4809 | SHB |

TABLE 6. Existence and stability of steady states according to $S_{in}$.

| Interval of $S_{in}$ | $\mathcal{E}_0$ | $\mathcal{E}_1$ | $\mathcal{E}^*$ |
|---|---|---|---|
| $(0, \sigma_1)$ | S | | |
| $(\sigma_1, \sigma_2)$ | U | S | |
| $(\sigma_2, \sigma_3)$ | U | U | S |
| $(\sigma_3, \sigma_4)$ | U | U | U |
| $(\sigma_4, \sigma_5)$ | U | U | S |
| $(\sigma_5, +\infty)$ | U | U | U |

Fig. 5 represents the one-parameter bifurcation diagram of system (1) where the $\omega$-limit set is projected in coordinate $S$ depending on the control parameter $S_{in}$. Indeed, in Fig. 5(a), we observe more clearly the transcritical bifurcations occurring at $\sigma_1$ and $\sigma_2$, and the occurrence of a stable limit cycle via a supercritical Hopf bifurcation at $\sigma_3$ and then their disappearance via a second supercritical Hopf bifurcation at $\sigma_4$. Once again, increasing further $S_{in}$, a stable limit cycle emerges through a supercritical Hopf bifurcation at $\sigma_5$ as shown in Fig. 5(b). Then, the oscillations are sustained for all $S_{in} > \sigma_5$.

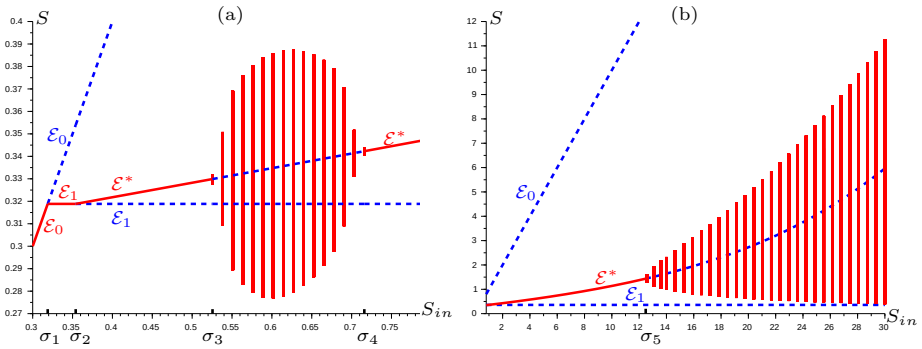


FIGURE 5. Scilab simulation showing projections of the $\omega$-limit set in variable $S$ when $D = 0.25$: (a) emergence and the disappearance of limit cycle at $\sigma_3$ and $\sigma_4$ for $S_{in} \in [0.3, 0.8]$; (b) emergence of limit cycle at $\sigma_5$ for $S_{in} \in [0.8, 30]$.

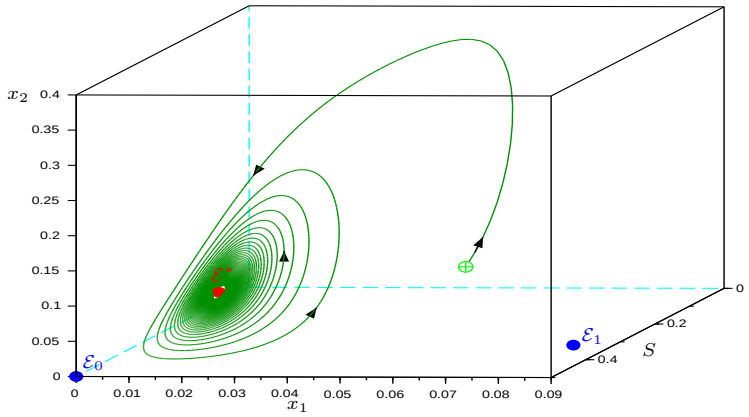


FIGURE 6. Case $S_{in} = 0.5 \in ]\sigma_2, \sigma_3[$ and $D = 0.25$: convergence to $\mathcal{E}^*$.

For the numerical simulations, we have used Maple [31] to plot the Figs. 1, 2, 4, 10, 11 and 12, MATCONT [32] for Fig. 3 and Scilab [38] for Figs. 5, 6, 7 and 8. The limit cycles in Figs. 5, 7 and 8 were plotted by solving the ordinary differential equations using the default solver "*lsoda*" from the ODEPACK package in Scilab. To validate the previous results, we illustrate in the following the three-dimensional phase plot and the trajectories over time in some interesting cases.

- For $S_{in} \in ]\sigma_2, \sigma_3[$, the numerical simulations done in the three-dimensional phase space $(S, x_1, x_2)$ for various positive initial conditions permit to conjecture the global convergence towards $\mathcal{E}^*$ (see Fig. 6).
- For $S_{in} \in ]\sigma_3, \sigma_4[$, the numerical simulations done for various positive initial conditions permit to conjecture the global asymptotic stability of a stable limit cycle (see Fig. 7).
- For $S_{in} > \sigma_5$, Fig. 8 shows the trajectory starting from a neighborhood of $\mathcal{E}^*$ of size order $\epsilon = 10^{-3}$ is approaching a stable limit cycle as time goes where the system exhibits sustained oscillations.

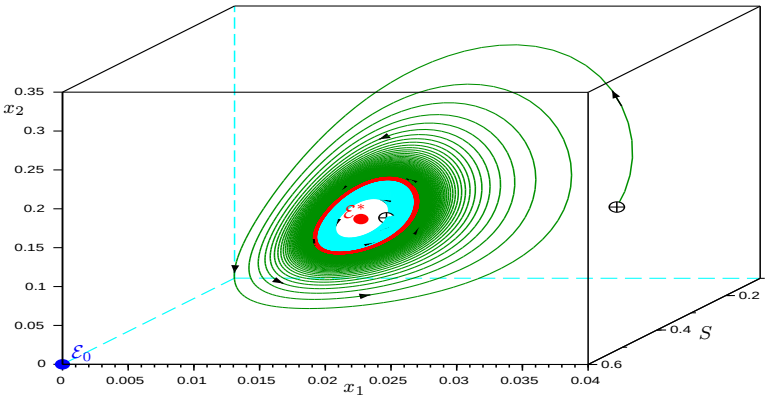


FIGURE 7. Case $S_{in} = 0.6 \in ]\sigma_3, \sigma_4[$ and $D = 0.25$: convergence towards a stable limit cycle (in red).

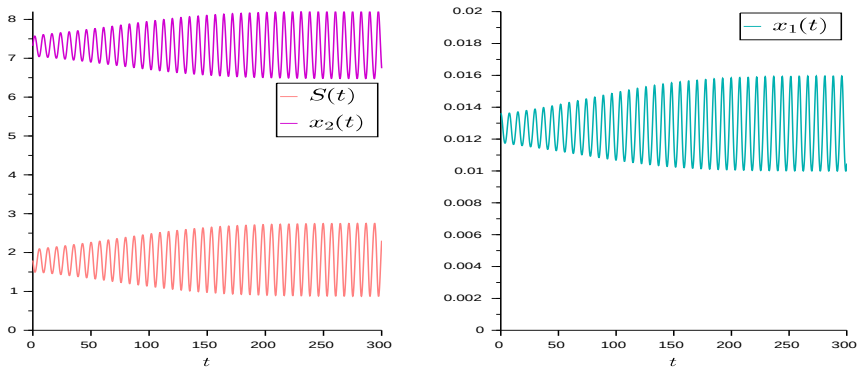


FIGURE 8. Case $S_{in} = 15 > \sigma_5$ and $D = 0.25$: convergence to a stable limit cycle showing the sustained oscillations.

5. **Conclusion.** In this paper, we have extended the mathematical analysis of the interspecific density-dependent model (1) describing a predator-prey relationship between two microbial species in a chemostat, by considering the effect of mortality with distinct disappearance rates. Using the nullcline method [15, 33], the necessary and sufficient conditions of existence of all steady states of (1) are determined according to the parameter control. Indeed, this method provides a geometric description of the existence of the boundary steady states which are unique and the multiplicity of the positive steady states For the local stability of the positive steady state, we have used the Routh–Hurwitz criterion (26) since we cannot determine explicitly the eigenvalues of the Jacobian matrix at this point, in contrast to the boundary steady states, the stability conditions are determined explicitly. We show that the positive steady state can destabilize with emergence of a stable limit cycle via a supercritical Hopf bifurcation.

Using the necessary and sufficient conditions of existence and stability of all steady states, the operating diagrams are analyzed analytically to determine the behavior of the system according to the concentration of substrate in the feed bottle $S_{in}$ and the dilution rate $D$. These conditions are plotted in MAPLE using specific growth functions given by (22). Then, these theoretically results on the operating diagram are validated numerically using MATCONT.

In fact, the process exhibits an even richer set of possible behaviors illustrated in the operating diagram: either the washout ($\mathcal{J}_1$) or the exclusion of the predator ($\mathcal{J}_2$) or the coexistence of the predator-prey species around a positive steady state ($\mathcal{J}_3$) or a stable limit cycles ($\mathcal{J}_4$) The one-parameter bifurcation diagram is determined according to the input substrate concentration $S_{in}$ as the bifurcating parameter. It shows the transcritical bifurcation as well as the three supercritical Hopf bifurcations with the appearance and the disappearance of the stable periodic orbits. The numerical simulations illustrate the three-dimensional phase space showing the coexistence around a coexistence steady state or a stable limit cycle, while the time course shows the sustained oscillations.

The comparison of our results with those in the existing literature [12, 33] proves that the addition of mortality terms of the species in the interspecific density-dependent model (1) with a predator-prey relationship can destabilize the positive steady states but not the global behavior of the process where the mortality of

species could lead to the occurrence of stable limit cycles with the coexistence of species.

## Appendix A. Proofs.

**Proof of Proposition 1.** Since the vector field defined by (1) is $C^1$, the uniqueness of a solution to initial value problems holds. From (1), for $i = 1, 2$,

$$x_i(t_0) = 0, \text{ for any } t_0 \geqslant 0 \quad \Longrightarrow \quad \dot{x}_i = 0.$$

If $x_i(0) = 0$, then $x_i(t) = 0$ for all $t$ since the boundary face where $x_i \equiv 0$ is invariant in the vector field $C^1$ by system (1). If $x_i(0) > 0$, then $x_i(t) > 0$ for all $t$ since $x_i \equiv 0$ cannot be reached in finite time by trajectories such that $x_i(0) > 0$ by the uniqueness of solutions. On the other hand, one has

$$S(t_0) = 0, \quad \text{for any } t_0 \geqslant 0 \quad \Longrightarrow \quad \dot{S}(t_0) = DS_{in} > 0.$$

Consequently, we have $S(t) \geqslant 0$ for all $t$. In fact, assume that $S(0) \geqslant 0$ and that it exists $t_0 > 0$, such that $S(t_0) = 0$ and $S(t) > 0$ for $t \in (0, t_0)$. Then, $\dot{S}(t_0) \leqslant 0$ 0) which contradicts $\dot{S}(t_0) > 0$. Therefore, the solutions remain non-negative. Let $z = S + x_1 + x_2$. From system (1), we have

$$\dot{z} = D(S_{in} - S) - D_1 x_1 - D_2 x_2.$$

Consequently,

$$\dot{z} \leqslant D_{\min}(DS_{in}/D_{\min} - z).$$

Using Gronwall's lemma, we obtain

$$z(t) \leqslant DS_{in}/D_{\min} + (z(0) - DS_{in}/D_{\min})e^{-D_{\min}t} \quad \text{for all} \quad t \geqslant 0. \tag{23}$$

We deduce that

$$z(t) \leqslant \max(z(0), DS_{in}/D_{\min}) \quad \text{for all} \quad t \geqslant 0.$$

Therefore, the solutions of (1) are positively bounded and are defined for all $t \geqslant 0$. From (23), we deduce that the set $\Omega$ is positively invariant and is a global attractor for (1). □

**Proof of Proposition 2.** For $\mathcal{E}_1$, $x_1 > 0$ and $x_2 = 0$. From the second equation of (3) and the definition (4) of the break-even concentration, it follows that $S = \lambda_1(D)$. From the first equation of (3), we obtain the $x_1$ component. Thus, $\mathcal{E}_1$ exists if and only if $x_1 > 0$, that is, condition (6) holds. □

**Proof of Proposition 5.** Using the notation (12), the Jacobian matrix of (1) at $(S, x_1, x_2)$ corresponds to the $3 \times 3$ matrix:

$$J = \begin{bmatrix} -D - Ex_1 - x_2F & -f_1(S, x_2) - Hx_2 & Gx_1 - f_2(S, x_1) \\ Ex_1 & f_1(S, x_2) - D_1 & -Gx_1 \\ Fx_2 & Hx_2 & f_2(S, x_1) - D_2 \end{bmatrix}.$$

For $\mathcal{E}_0 = (S_{in}, 0, 0)$, the eigenvalues are the roots of the following characteristic polynomial

$$P(\lambda) = (\lambda + D)(\lambda + D_2)(\tilde{\lambda}_1 - \lambda)$$

where $\tilde{\lambda}_1 = f_1(S_{in}, 0) - D_1$. Thus, $\mathcal{E}_0$ is LES if and only if $f_1(S_{in}, 0) < D_1$, that is, $S_{in} < \lambda_1(D)$.

For $\mathcal{E}_1 = (\lambda_1(D), \tilde{x}_1, 0)$, the characteristic polynomial is

$$P(\lambda) = (\tilde{\lambda}_1 - \lambda)(\lambda^2 + c_1\lambda + c_2)$$

where $\tilde{\lambda}_1 = \widetilde{f}_2(\tilde{x}_1, 0)$, $c_1 = D + \tilde{x}_1 E$ and $c_2 = D_1 \tilde{x}_1 E$. Since $c_1 > 0$ and $c_2 > 0$, the real parts of the roots of the quadratic factor are negative. Therefore, $\mathcal{E}_1$ is LES if and only if $\widetilde{f}_2(\tilde{x}_1, 0) < 0$, that is, condition (18) holds.

For $\mathcal{E}^* = (S^*, x_1^*, x_2^*)$, the characteristic polynomial is

$$P(\lambda) = \lambda^3 + c_1\lambda^2 + c_2\lambda + c_3, \tag{24}$$

where

$$\begin{aligned} &c_1 = D + Ex_1^* + Fx_2^*, \quad c_2 = D_1 Ex_1^* + D_2 Fx_2^* + (GH + EH - FG)x_1^* x_2^* \\ &c_3 = (DGH + D_2 EH - D_1 FG)x_1^* x_2^*. \end{aligned} \tag{25}$$

Since $c_1 > 0$, according to the Routh–Hurwitz criterion, $\mathcal{E}^*$ is LES if and only if

$$c_3 > 0 \quad \text{and} \quad c_4(S_{in}, D) = c_1 c_2 - c_3 > 0 \tag{26}$$

where the function $c_4$ can be written as its expression (21). Using the expressions of $F_1'$ in (13) and of $F_2'$ in (15), we obtain

$$F_1'(x_1) - F_2'(x_1) = \frac{D_1 FG - D_2 EH - DGH}{D_2 F(D_2 E/D + G)}.$$

Consequently, at $\mathcal{E}^*$, we have

$$c_3 = \left(F_2'(x_1^*) - F_1'(x_1^*)\right) D_2 F[D_2 E/D + G]x_1^* x_2^*. \tag{27}$$

Thus, $E^*$ is LES if and only if $F_2'(x_1^*) > F_1'(x_1^*)$ and condition (21) holds. □

**Appendix** B. **Construction of the operating diagrams in Fig. 2.** In this section, we present the method used to construct theoretically the operating diagrams presented in Fig. 2. To this end, we plot the various curves from the existence and stability conditions which depend on the operating parameters. In addition, we will see in the following that the proof is based on the existence and stability conditions in Table 1 and is supported by numerical experimentation when the biological parameter values are fixed in Table 7. From Table 1, the steady state $\mathcal{E}_0$ always exists and is stable if and only if $S_{in} < \lambda_1(D)$, that is, it is stable in the region bounded by the curve $\Upsilon_1$ and located above this curve, see Fig. 2. The steady state $\mathcal{E}_1$ exists in the region bounded by the curve $\Upsilon_1$ and located below this curve and is stable in the region bounded by the curve $\Upsilon_2$ and located at the left of this curve. The steady state $\mathcal{E}^*$ exists in the region bounded by the curve $\Upsilon_2$ and located at the right of this curve. To determine the sign of $c_3(S_{in}, D)$ in the operating diagram and the curve $\Upsilon_3$ defined by $c_4(S_{in}, D) = 0$, we use the concept of *steady-state characteristic* which we apply in the following as in [17]. A positive steady state $\mathcal{E}^* = (S^*, x_1^*, x_2^*)$ is a solution of the set of equations

$$\begin{cases} D(S_{in} - S) &= D_1 x_1 + D_2 x_2, \\ f_1(S, x_2) &= D_1, \\ f_2(S, x_1) &= D_2. \end{cases} \tag{28}$$

From the second and the third equations of (28), we can define the solutions $x_2$ and $x_1$, respectively, as functions of $S$, that is, there exist $S \longmapsto X_2(S)$ and $S \longmapsto X_1(S)$ such that

$$f_1(S, X_2(S)) = D_1 \quad \text{and} \quad f_2(S, X_1(S)) = D_2.$$

More precisely, let $S \geqslant 0$. From (H2), the function $x_2 \mapsto f_1(S, x_2)$ is decreasing. Thus, the equation $f_1(S, x_2) = D_1$ has a unique solution $x_2 = X_2(S)$ if and only if

$$f_1(S, +\infty) < D_1 \leqslant f_1(S, 0), \quad \text{that is,} \quad S \in I_1 = [\lambda_1, \lambda_1'),$$

where $\lambda_1$ is defined by (4) and $\lambda_1'$ is the unique solution, if it exits, of the equation

$$f_1(S, +\infty) = D_1.$$

If $D_1 > f_1(S, +\infty)$ for all $S \geqslant 0$, then we put $\lambda_1' = +\infty$. Note that the function $X_2(\cdot)$ is increasing and satisfies $X_2(\lambda_1) = 0$ and $X_2(\lambda_1') = +\infty$. From (H1) and (H2), the function $x_1 \mapsto f_2(S, x_1)$ is increasing and $f_2(S, 0) = 0$. Hence, the equation $f_2(S, x_1) = D_2$ has a unique solution $x_1 = X_1(S)$ if and only if

$$D_2 < f_2(S, +\infty), \quad \text{that is,} \quad S > \lambda_2',$$

where $\lambda_2'$ is the unique solution, if it exits, of the equation

$$f_2(S, +\infty) = D_2.$$

If $D_2 > f_2(S, +\infty)$ for all $S \geqslant 0$, then we put $\lambda_2' = +\infty$. Note that the function $X_1(\cdot)$ is decreasing and satisfies $X_1(\lambda_2') = +\infty$.

Let $C_j(S)$, $j = 3, 4$ be the functions defined by the same formulas as (25) and (26), respectively, where the functions $E$, $F$, $G$ are $H$ in these functions depends only on $x_1$, $x_2$ and $S$. But, as the $x_i = X_i(S)$, $i = 1, 2$, then these functions $C_j$ depend only on $S$. More precisely, we have

$$c_j(S_{in}, D) = C_j(S^*(S_{in}, D)), \quad j = 3, 4.$$

where $S^*(S_{in}, D)$ is the solution of equation

$$D(S_{in} - S) = H(S) := D_1 X_1(S) + D_2 X_2(S). \tag{29}$$

Fig. 9 illustrates that the function $C_3(S)$ is positive for various values of $D$ from the starting points in red of coordinates $(\max(\lambda_1(D), \lambda_2'(D)), 0)$. Note that for the specific growth rates (22), $\lambda_1' = +\infty$ since $D_1 > f_1(S, +\infty) = 0$ for all $S \geqslant 0$. According to expression (27), this positivity of $C_3(S)$ for any value of $D$ in its definition domain shows that $F_2'(x_1^*) > F_1'(x_1^*)$ for this set of parameters in Table 7. Thus, system (1) cannot exhibits a multiplicity of positive steady states appearing through saddle-node bifurcations and other regions in the operating diagram.

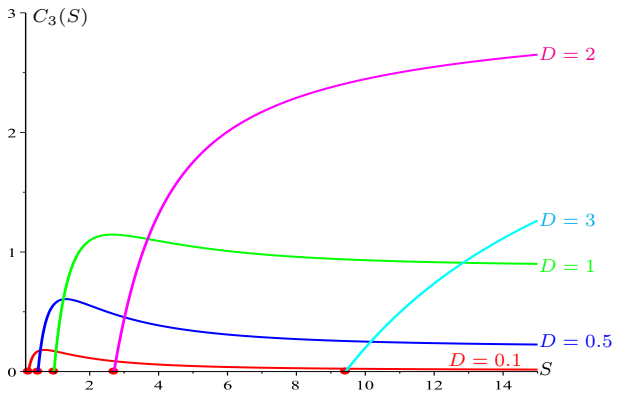


FIGURE 9. Curves of the function $C_3(S)$ for different values of $D$ when $S > \max(\lambda_1(D), \lambda_2'(D))$.

In Fig. 10, the curve of the function $H(S)$ is colored in blue when $C_4(S) < 0$, that is, when the positive steady state is unstable. It is colored in red when $C_4(S) > 0$, that is, when the positive steady state is stable. From (29), the critical value of $S_{in}$

corresponding to Hopf bifurcation when $C_4(S) = 0$ (or also when the curve of $H(S)$ changes color) is given by

$$S_{in} = H(S)/D - S.$$

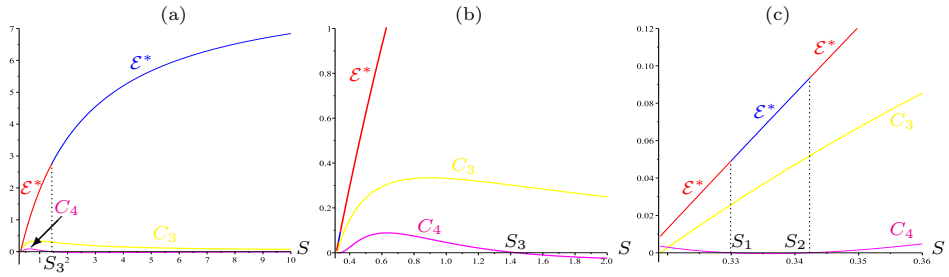


FIGURE 10. (a) Steady-state characteristics describing the local asymptotic behavior of the positive steady state $\mathcal{E}^*$ when $D = 0.25$. Magnification for (b) $S \leqslant 2$ and (c) $0.32 \leqslant S \leqslant 0.36$.

In particular, if the equation $C_4(S) = 0$ has $n$ solutions $S_i$, for $i = 1, \ldots, n$, with $n$ is the number of solutions, we have

$$\sigma_{i+2} = H(S_i)/D - S_i. \tag{30}$$

Finally, using a procedure in $D$, we can determine the curve $\Upsilon_3$ corresponding to Hopf bifurcation in the operating diagram of Fig. 2.

For the set of parameters in Table 7 corresponding to the operating diagram in Fig. 2, the numerical simulations show that the equation $C_4(S) = 0$ has three solutions $S_i$, $i = 1, 2, 3$ for $0 < D < D^* \simeq 0.2648$ (see Fig. 11). Using (30), we can deduce the corresponding three critical values $\sigma_i$, $i = 3, 4, 5$, which are provided in Table 5 and shown in Fig. 5. Moreover, these critical values correspond to the curve $\Upsilon_3$ in Fig. 2. However, when $D^* < D < D_{\max} \simeq 1.595$, the equation $c_4(S) = 0$ has a unique solution $S_1$ that corresponds to the unique critical value $\sigma_3$.

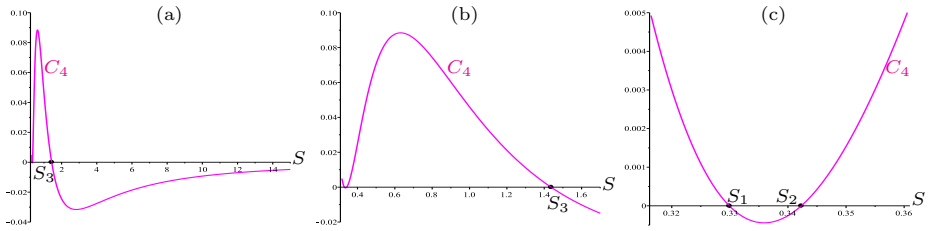


FIGURE 11. Case $D = 0.25 \leqslant D^* \simeq 0.2648$: (a) Change of sign of $C_4$ when $S_1 \simeq 0.3299$ (or equivalently $\sigma_3 \simeq 0.5255$), $S_2 \simeq 0.3423$ (or equivalently $\sigma_4 \simeq 0.7159$) and $S_3 \simeq 1.4365$ (or equivalently $\sigma_5 \simeq 12.4809$). (b)-(c) Magnifications for $S \in [0.316, 1.7]$ and $S \in [0.316, 0.361]$.

**Appendix** C. **Numerical evidence of the Hopf bifurcation.** To understand and analyze the change of local stability occurring through the positive steady state $\mathcal{E}^*$ as $S_{in}$ varies, we determine numerically the eigenvalues of the Jacobian matrix $\mathcal{J}$ at $\mathcal{E}^*$ by solving the roots of the characteristic polynomial (24). Indeed,

this characteristic polynomial has one negative eigenvalue and one pair of complex-conjugate eigenvalues

$$\bar{\lambda}_j = \mu(S_{in}) \pm i\nu(S_{in}), \quad j = 1, 2. \tag{31}$$

Increasing the operating parameter $S_{in}$, this pair (31) crosses the imaginary axis first at the critical values $\sigma_3$ from negative to positive half plane and second it returns to the negative half plane at $\sigma_4$ and finally it returns again to the positive half plane at $\sigma_5$ (see Fig. 12), that is, it becomes purely imaginary for $\sigma_i$, $i = 3, 4, 5$ such that $\mu(\sigma_i) = 0$, with $\nu(\sigma_i) \neq 0$. In addition, numerically, we check the following inequality

$$\frac{d\mu}{dS_{in}}(\sigma_i) \neq 0, \quad i = 3, 4, 5. \tag{32}$$

This is consistent with Fig. 5, showing that, as $S_{in}$ increases and crosses $\sigma_i$, $i = 3, 4, 5$, the positive steady state $\mathcal{E}^*$ changes its stability through three supercritical Hopf bifurcations with the occurrence or disappearance of a stable limit cycle that we illustrate in Figs. 7 and 8.

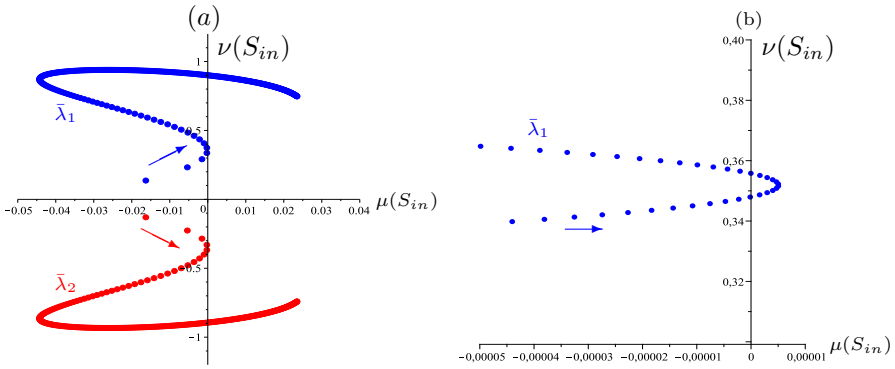


FIGURE 12. (a) Variation of the pair of complex-conjugate eigenvalues (31) as $S_{in}$ increases from 0 to 40 when $D = 0.25$. (b) Magnification on $\bar{\lambda}_1$ for $S_{in} \in [0.4, 0.8]$.

**Appendix** D. **Parameter values used for numerical simulations.** All the values of the parameters used in the numerical simulations are provided in Table 7.

TABLE 7. Parameter values used for model (1) when the growth rates $f_1$ and $f_2$ are given by (22).

| Parameter | $m_1$ | $K_1$ | $L_1$ | $m_2$ | $K_2$ | $L_2$ | $\alpha_1$ | $\alpha_2$ | $a_1$ | $a_2$ |
|---|---|---|---|---|---|---|---|---|---|---|
| Fig. 1(c) | 2.75 | 2 | 1.2 | 2.95 | 1.8 | 1.5 | $10^{-3}$ | 0.1 | 0.95 | 0.7 |
| Figs. 1(a,b),2,3,5–12 | | | | | | | | | 0.3 | 0.2 |
| Fig. 4(a) | 4 | 2 | 3 | 8 | 0.1 | 0.2 | 1 | 1 | 0.3 | 0.05 |
| Fig. 4(b) | | | | | | | | | 0.1 | 0.05 |
| Fig. 4(c) | | | | | | | | | 0 | 0 |

## REFERENCES


[1] N. Abdellatif, R. Fekih-Salem and T. Sari, Competition for a single resource and coexistence of several species in the chemostat, *Math. Biosci. Eng.*, *13* (2016), 631–652.

[2] M. Ballyk, R. Staffeldt and I. Jawarneh, A nutrient-prey-predator model: Stability and bifurcations, *Discrete & Continuous Dyn. Syst. - S*, *13* (2020), 2975–3004.

[3] B. Bar and T. Sari, The operating diagram for a model of competition in a chemostat with an external lethal inhibitor, *Discrete & Continuous Dyn. Syst. - B*, **25** (2020), 2093–2120.

[4] B. Benyahia, T. Sari, B. Cherki and J. Harmand, Bifurcation and stability analysis of a two step model for monitoring anaerobic digestion processes, *J. Proc. Control*, **22** (2012), 1008–1019.

[5] O. Bernard, Z. Hadj-Sadok, D. Dochain, A. Genovesi and J-P. Steyer, Dynamical model development and parameter identification for an anaerobic wastewater treatment process, *Biotechnol. Bioeng.*, **75** (2001), 424–438.

[6] M.P. Boer, B.W. Kooi and S.A.L.M. Kooijman, Food chain dynamics in the chemostat, *Math. Biosci.*, **150** (1998), 43–62.

[7] F. Borsali and K. Yadi, Contribution to the study of the effect of the interspecificity on a two nutrients competition model, *Int. J. Biomath.*, **8** (2015), 1550008, 17 pp.

[8] Y. Daoud, N. Abdellatif, T. Sari, and J. Harmand, Steady state analysis of a syntrophic model: The effect of a new input substrate concentration, *Math. Model. Nat. Phenom.*, **13** (2018), 1–22.

[9] P. De Leenheer, D. Angeli and E.D. Sontag, Crowding effects promote coexistence in the chemostat, *J. Math. Anal. Appl.*, **319** (2006), 48–60.

[10] M. Dellal and B. Bar, Global analysis of a model of competition in the chemostat with internal inhibitor, *Discrete & Continuous Dyn. Syst. - B*, **26** (2021), 1129–1148.

[11] M. Dellal, M. Lakrib and T. Sari, The operating diagram of a model of two competitors in a chemostat with an external inhibitor, *Math. Biosci.*, **302** (2018), 27–45.

[12] M. El-Hajji, How can inter-specific interferences explain coexistence or confirm the competitive exclusion principle in a chemostat?, *Int. J. Biomath.*, **11** (2018), 1850111, 20 pp.

[13] M. El-Hajji, F. Mazenc and J. Harmand, A mathematical study of a syntrophic relationship of a model of anaerobic digestion process, *Math. Biosci. Eng.*, **7** (2010), 641–656.

[14] R. Fekih-Salem, J. Harmand, C. Lobry, A. Rapaport and T. Sari, Extensions of the chemostat model with flocculation, *J. Math. Anal. Appl.*, **397** (2013), 292–306.

[15] R. Fekih-Salem, C. Lobry and T. Sari, A density-dependent model of competition for one resource in the chemostat, *Math. Biosc.*, **268** (2017), 104–122.

[16] R. Fekih-Salem, A. Rapaport and T. Sari, Emergence of coexistence and limit cycles in the chemostat model with flocculation for a general class of functional responses, *Appl. Math. Modell.*, **40** (2016), 7656–7677.

[17] R. Fekih-Salem and T. Sari, Properties of the chemostat model with aggregated biomass and distinct removal rates, *SIAM J. Appl. Dyn. Syst. (SIADS)*, **18** (2019), 481–509.

[18] R. Fekih-Salem and T. Sari, Operating diagram of a flocculation model in the chemostat, *ARIMA J.*, **31** (2020), 45–58.

[19] B. Haegeman and A. Rapaport, How flocculation can explain coexistence in the chemostat, *J. Biol. Dyn.*, **2** (2008), 1–13.

[20] S.R. Hansen and S.P. Hubbell, Single-nutrient microbial competition: Qualitative agreement between experimental and theoretically forecast outcomes, *Science*, (1980), 1491–1493.

[21] J. Harmand, C. Lobry, A. Rapaport and T. Sari, The Chemostat: Mathematical Theory of Microorganism Cultures, vol. 1, *Chemical Eng. Ser., Chemostat Bioprocesses Set, Wiley, New York.*, (2017).

[22] J. Harmand, A. Rapaport, D. Dochain and C. Lobry, Microbial ecology and bioprocess control: Opportunities and challenges, *Journal of Process Control*, **18** (2008), 865–875.

[23] S.-B. Hsu, C.A. Klausmeier and C.-J. Lin, Analysis of a model of two parallel food chains, *Discrete & Continuous Dyn. Syst. - B*, **12** (2009), 337–359.

[24] Z. Khedim, B. Benyahia, B. Cherki, T. Sari and J. Harmand, Effect of control parameters on biogas production during the anaerobic digestion of protein-rich substrates, *Appl. Math. Model.*, **61** (2018), 351–376.

[25] B.W. Kooi and M.P. Boer, Chaotic behaviour of a predator-prey system in the chemostat, *Dyn. Contin. Discrete Impuls. Syst. Ser. B Appl. Algorithms*, **10** (2003), 259–272.

[26] B. Li and Y. Kuang, Simple food chain in a chemostat with distinct removal rates, *J. Math. Anal. Appl.*, **242** (2000), 75–92.
[27] C. Lobry and J. Harmand, A new hypothesis to explain the coexistence of n species in the presence of a single resource, *C. R. Biol.*, **329** (2006), 40–46.
[28] C. Lobry and F. Mazenc, Effect on persistence of intra-specific competition in competition models, *Electron. J. Diff. Equ.*, **125** (2007), 1–10.
[29] C. Lobry, F. Mazenc and A. Rapaport, Persistence in ecological models of competition for a single resource, *C. R. Acad. Sci. Paris, Ser. I*, **340** (2005), 199–204.
[30] C. Lobry, A. Rapaport and F. Mazenc, Sur un modèle densité-dépendant de compétition pour une ressource, *C. R. Biol.*, **329** (2006), 63–70.
[31] MAPLE [Software], Version 13.0, *Maplesoft, a division of Waterloo Maple Inc., Waterloo, Ontario.*, (2009).
[32] MATCONT [Software]. *https://sourceforge.net/projects/matcont/?source=directory.*
[33] T. Mtar, R. Fekih-Salem and T. Sari, Interspecific density-dependent model of predator-prey relationship in the chemostat, *Int. J. Biomath.*, **14** (2021), 2050086, 22 pp.
[34] T. Mtar, R. Fekih-Salem and T. Sari, Effect of the mortality on a density-dependent model with a predator-prey relationship, *CARI'2020, Proceedings of the 15th African Conference on Research in Computer Science and Applied Mathematics*, (2020).
[35] A. Rapaport and M. Veruete, A new proof of the competitive exclusion principle in the chemostat, *Discrete & Continuous Dyn. Syst. - B*, **24** (2019), 3755–3764.
[36] T. Sari and J. Harmand, A model of a syntrophic relationship between two microbial species in a chemostat including maintenance, *Math. Biosci.*, **275** (2016), 1–9.
[37] M. Sbarciog, M. Loccufier and E. Noldus, Determination of appropriate operating strategies for anaerobic digestion systems, *Biochem. Eng. J.*, **51** (2010), 180–188.
[38] SCILAB [Software], version 6.0.1, *Scilab Enterprises SAS.*, (2018).
[39] S. Shen, G.C. Premier, A. Guwy, and R. Dinsdale, Bifurcation and stability analysis of an anaerobic digestion model, *Nonlinear Dynam.*, **48** (2007), 391–408.
[40] H.L. Smith and P. Waltman, The Theory of the Chemostat, Dynamics of Microbial Competition, *Cambridge University Press*, (1995).
[41] G.A.K. Van Voorn, B.W. Kooi and M.P. Boer, Ecological consequences of global bifurcations in some food chain models, *Math. Biosci.*, **226** (2010), 120–133.
[42] D.V. Vayenas and S. Pavlou, Chaotic dynamics of a food web in a chemostat, *Math. Biosci.*, **162** (1999), 69–84.
[43] M.J. Wade and R.W. Pattinson and N.G. Parker and J. Dolfing, Emergent behaviour in a chlorophenol-mineralising three-tiered microbial 'food web', *J. Theor. Biol.*, **389** (2016), 171–186.
[44] M. Weedermann, G.S.K. Wolkowicz and J. Sasara, Optimal biogas production in a model for anaerobic digestion, *Nonlinear Dyn.*, **81** (2015), 1097–1112.
[45] G.S.K. Wolkowicz, Successful invasion of a food web in a chemostat, *Math. Biosci.*, **93** (1989), 249–268.
[46] A. Xu, J. Dolfing, T.P. Curtis, G. Montague and E. Martin, Maintenance affects the stability of a two-tiered microbial 'food chain'?, *J. Theor. Biol.*, **276** (2011), 35–41.

*E-mail address*: tahani.mtar@enit.utm.tn
*E-mail address*: radhouene.fekihsalem@isima.rnu.tn
*E-mail address*: tewfik.sari@inrae.fr